Journal of Molecular Graphics and Modelling 83 (2018) 112–121

Contents lists available at ScienceDirect

Journal of Molecular Graphics and Modelling

journal homepage: www.elsevier.com/locate/JMGM

Revealing the molecular interactions of aptamers that specifically bind to the extracellular domain of HER2 cancer biomarker protein: An *in silico* assessment

Sarfaraj Niazi [a, **], Madhusudan Purohit [a], Archana Sonawani [b], Javed H. Niazi [c, *]

[a] Department of Pharmaceutical Chemistry, JSS College of Pharmacy-Mysuru, JSS Academy of Higher Education and Research, Mysuru, 570015, India
[b] Biomedical Informatics Centre of ICMR, National Institute for Research in Reproductive Health, JM Street, Parel, Mumbai, 400012, India
[c] Sabanci University Nanotechnology Research Centre (SUNUM), Orta Mh., 34956, Tuzla, Istanbul, Turkey

ARTICLE INFO

Article history:
Received 1 May 2018
Received in revised form
3 June 2018
Accepted 4 June 2018
Available online 6 June 2018

Keywords:
Aptamers
Cancer therapeutics
Cancer diagnostics
HER2
In silico
Docking
MD simulations
SELEX

ABSTRACT

Single-stranded (ss) oligonucleotide aptamers are emerging as the promising substitutes for monoclonal antibodies because of their low production cost and good batch-to-batch consistency. Aptamers vividly bind to a variety of cellular targets and alter their functions with a remarkable degree of specificities. In this study, the positive clones of human epidermal growth factor receptor 2 (HER2) specific binding ssDNA aptamers which were previously identified by *in vitro* Systematic Evolution of Ligands by EXponential enrichment (SELEX) process, hitherto lacking the putative binding site information and residues crucial for aptamer recognition are studied. Primarily, four putative DNA binding regions present on the HER2 extracellular domain (ECD) were identified using prediction servers and electrostatic potential maps, which were further exploited to delineate the aptamer binding features. Molecular docking and molecular dynamics (MD) simulations revealed stable binding nature of three aptamers (H2>H1>H6), which chose *Site 2a* as preferred binding site present on the HER2(ECD) protein. Furthermore, amino acid residues *viz.* Asn37, Gln59, Arg81-Gln84, Asp88, and Lys128 of *Site 2a* were found to be crucial for high-affinity binding. This knowledge can be utilized as a benchmark for the future studies, in search for better and highly specific anti-HER2 aptamers as cancer therapeutics or as diagnostic agents.

1. Introduction

Human epidermal growth factor receptor 2 (HER2), also known as CD340 or ErbB2, is an important member of epidermal growth factor receptor family. A tight regulation of HER2 signaling is a prerequisite for the normal growth and development of the cells. Structurally, HER2 is constituted by three distinct domains, namely, N-terminal extracellular domain (ECD), a transmembrane domain (TMD) and cytoplasmic tyrosine kinase domain with C-terminal tail [1,2]. The HER2(ECD) consists of 4 sub-domains (I to IV) which are amenable to conformational changes due to interconnected flexible loops and play active roles in receptor activation. In an open conformation, the juxtaposition of sub-domain I and sub-domain III of HER2(ECD) make sub-domain II - a dimerization domain, “open” to interact with other HER monomers. Whereas, sub-domain III adjoins sub-domain IV and extends to a single α-helical TMD, which in turn connect to the intracellular tyrosine kinase domain through a small cytoplasmic juxta-membrane segment [3,4]. Initiation of HER2 downstream signaling cascade is attributed to its dimerization with structurally related HERs namely, HER1, HER3, and HER4, which can exist as either homo or heterodimer form. The orphan and constitutively active HER2 monomer dimerize with another monomer of its kind, or any of the ligand bound active HER1/HER3/HER4 monomers [4,5]. Among these pairs, HER2-HER3 dimerization induces the highest intrinsic activity [6]. Dimerization initiates a cascade of downstream signaling events such as activation of mitogen-activated protein kinase (MAPK), phosphoinositide 3-kinase (PI-3K)/Akt and Ca^{2+} signaling pathways [7]. These events cause increased cell division, decreased apoptosis and increased cell survival rate.

Over the past three decades, since the discovery of HER2 as an

* Corresponding author.
** Corresponding author.
E-mail addresses: sarfarajniazi@jssuni.edu.in, sarfarazkolkar@gmail.com (S. Niazi), javed@sabanciuniv.edu (J.H. Niazi).

https://doi.org/10.1016/j.jmgm.2018.06.003
1093-3263/

oncogene, a significant progress has been achieved, especially in the cancer prognosis and treatment [8]. It is now a well-established fact that HER2 overexpression is associated with ~20–30% of aggressive breast cancer cases and several other types of cancers including ovarian, lung, gastric and oral cancers [9,10]. Hence, several attempts have been made to develop small molecules that may serve as HER2-targeted therapeutics for cancer and/or biomarkers for the early diagnosis.

Several synthetic small molecule inhibitors of the intracellular HER2-kinase domain have been developed. Some of the well-known potent inhibitors of HER2 kinase domain are, GW572016 (Lapatinib) [11,12], CI-1033 (Canertinib) [13], HKI-272 (Neratinib) [14], AEE-788 [15], BIBW-2992 (Afatinib) [16], BMS-599626 [17], ZD1839 (Gefitinib) [18], and CP-724714 [19] whose IC_{50} values range from 0.5 nM to 60 nM. Monoclonal antibodies such as, Pertuzumab [20], Trastuzumab [21], scFv chA21 [22], Fab37 [23], Affibody zHER2 [24] have been designed to target HER2(ECD). Recently, the structurally engineered ankyrin repeat proteins-DRPin G3, DRPin 9.29 [25] were developed which targets the extracellular domain of the HER2 protein (Fig. S1).

The discovery of ssDNA aptamers that specifically bind to the HER2 protein holds immense promise because of their low production cost and better batch-to-batch consistency as compared to the protein therapeutics. Therefore, aptamers could serve as a better substitute for the existing HER2 inhibitors. In the light of this conception, earlier we reported seven aptamers (H1-H7) that specifically bind to the HER2 protein [26]. Also, an *in vitro* assay method was developed for the detection of HER2 protein in the human serum using H2 aptamer as a prototype candidate [26]. Nevertheless, further study necessitates a detailed *in silico* structural characterization of the shortlisted aptamers (H1-H7) in the realm of molecular interactions, and assessment of their relative binding affinity for HER2 protein using molecular docking and MD simulations. Therefore, in the present study, combinations of *in silico* techniques are employed to extrapolate the nature of aptamer-protein interactions and thus advancing the functionality of the aptamers.

2. Materials and methods

2.1. Structural modeling of HER2(ECD)

The X-ray crystal structure of HER2(ECD) was retrieved from RCSB Protein Data Bank (PDB ID: 1N8Z resolution: 2.5 Å; UniProt ID: P04626) [21]. Missing 3D structural coordinates corresponded to the residue sequences *viz.* Asn102-Ala110, Glu303-Gly305, and Gly361-Ala364 (see sequence alignment; Fig. S2) were modeled using Build Homology Models protocol of BIOVIA Discovery studio 3.5 (DS. 3.5). Gap segments in the template were modeled by the integrated loop model tool and their geometry was refined by DOPE (Discrete Optimized Protein Energy) method. All the disulfide bridges and ligand groups in the template structure are kept intact and the optimization level was set to high. The side chains of the modeled regions were optimized using Side-Chain Refinement module of BIOVIA DS. 3.5 with the implementation of CHARMM force field. This was followed by 400 steps of global energy minimization using steepest descent method and Generalized Born as an implicit solvent model. The refined model was evaluated by SAVES server (https://services.mbi.ucla.edu/SAVES/). The data indicated that the model is reliable with 92.6% of residues in the most favored region from the Ramachandran plot, 92.38% ERRAT and 94.0% VERIFY 3D scores (Fig. S3). The validated model of HER2(ECD) was used for further *in silico* studies.

2.2. Prediction of putative DNA binding (DB) residues

The putative DB residues of HER2(ECD) were identified by using DISPLAR [27] and DNABINDPROT [28] structure-based DB residues prediction servers. Given the 3D structure of a protein as an input, the servers enable the use of prediction tools that used distinct algorithms to predict the potential DB residues. Prediction by DISPLAR is based on the neural networks, while the DNABINDPROT, uses the dynamic derived features of protein residues in high-fluctuation modes and their evolutionary conservation. In the present study, a consensus of these two distinct prediction algorithms is considered to garner the information of potential DB residues.

2.3. Generation of continuum electrostatic potential maps

The continuum electrostatic potential maps on the protein surfaces were generated by Adaptive Poisson-Boltzmann Solver (APBS) package [29] using AMBER99 force field implemented in the PDB2PQR web server ver. 2.0.0 [30]. The protonation states of titratable residues were assigned at pH 7.4 using PROPKA. Default values of dielectric constant (salute: 2 and solvent: 78.54) and temperature (298.15 K) were used for ABPS calculations. The continuum electrostatic potential maps of the solvent accessible surfaces were shown in dimensionless units of kT/*e*, where k is Boltzmann's constant, T is the temperature in Kelvin and *e* is the charge of an electron. The continuum electrostatic potential surfaces were rendered using PyMOL ABPS tool (Schrödinger, LLC. (2010)).

2.4. Structural modeling of variant regions of canonical anti-HER2 aptamers

3D structures of the truncated variant regions of the anti-HER2 aptamer along with poly T (Table 1) were modeled (from 3′ direction) using Build and Edit Nucleic Acid tool of DS. 3.5. The phosphate group at 5′ and oxygen atom at the 3′ termini of the aptamer varients were capped and primed with the hydroxyl group and a hydrogen atom, respectively in order to maintain neutral electronic milieu. All the modeled structures of the aptamers were subjected to energy minimization by steepest descent method using Generalized Born as an implicit solvent model with the implementation of CHARMM force field.

2.5. Aptamer-protein docking setup

The modeled structures of anti-HER2 aptamers along with a negative control poly T aptamer were docked to HER2(ECD) using HADDOCK web server protocol ver. 2.1 [31]. Prior to docking, constraints were included for the protein by assigning the DB residues predicted by DISPLAR and DNABINDPROT as active residues, while all the residual solvent-accessible residues were defined as passive. To define the docking constraints for anti-HER2 aptamers, all nucleotide bases of the seven aptamers were defined as active residues. Hence, a total of seven independent docking runs were carried out. The simulations were driven using the predefined docking constraints which were converted into ambiguous interaction restraints by HADDOCK. The docking protocol comprised of three stages, namely (a) rigid-body energy minimization, (b) semi-flexible refinement and (c) final model refinement in explicit solvent (TIP3P) model. A maximum of 200 water refined models (WRMs) obtained in the final stage of each docking run were clustered using a pair-wise backbone rmsd cut-off of 7.5 Å and a minimum cluster size of 4 as criteria. Several clusters were generated. These clusters were ranked on the basis of HADDOCK scores,

Table 1
Sequence information of anti-HER2 aptamers selected during the SELEX process along with a nonspecific poly T sequence.

Sr No.	Candidate No.	Anti-HER2 aptamer codes	Canonical anti-HER2 aptamers[a] (5′→3′)
1	1/13 [b]	H1	gggccgttcgaacacgagcatg**ggcggg**cctaggatgacctgagtctgtcc
2	6/10 [b]	H2	gggccgtcgaacacgagcatg**gtgcgtgga**cctaggatgacctgagtactgtcc
3	3	H3	gggccgttcgaacacgagcatg**gcgggt**cctaggatgacctgagtactgtcc
4	5	H4	gggccgttcgaacacgagcatg**ggtgcc**ctaggatgacctgagtactcc
5	2	H5	gggccgttcgaacacgagcatg**gggg**cctaggatgacctgagtactgtcc
6	8/9 [b]	H6	gggccgttcgaacacgagcat**gatac**ctaggatgacctgagtactgtcc
7	12	H7	gggccgttcgaacacgagcatg**ggtgtgaca**cctaggatgacctgagtactgtcc
8	Poly T[c]	Poly T	tttttt

[a] The variable regions (bold and underlined) of canonical anti-HER2 aptamer sequences are used to model 3D structures for the purpose of *In Silico* studies. The truncated anti-HER2 aptamers with a variable aptamer sequence length of three nucleotide bases were added with an additional residue overhang (bold and italicized) on either end to generate 3D models for *in silico* studies.
[b] These aptamers appeared multiple times during the *in vitro* SELEX process Ref. [26].
[c] Negative control.

which is the sum of weighted intermolecular energy terms such as, electrostatic (Elec), van der Waals (vdW), desolvation (Dsolv) and Ambiguous Interaction Restraints (AmIR) energies (equation (1)) [32]. While the rigid-body score is obtained by subtracting the HADDOCK score with the weighted (0.05) buried surface area (BSA) term.

$$\text{HADDOCK score} = 1.0 * \text{Elec} + 1.0 * \text{vdW} + 1.0 * \text{Dsolv} + 1.0 * \text{AmIR} \quad (1)$$

The results of cluster analysis obtained from eight independent docking runs (H1-H7 and poly T) are shown in Table 2 (see results section). The model belonged to the largest cluster having the best HADDOCK score was chosen as a representative of each docking run output.

2.6. Molecular dynamics (MD) simulations

100 ns MD simulations were performed for the four representative docked models *viz.* HER2(ECD)-H1, HER2(ECD)-H2, HER2(ECD)-H6 and HER2(ECD)-poly T. The simulations were performed using GROMACS ver. 4.5.4 [33] with the implementation of the CHARMM27 force field [34]. The topology files for all the aptamers were generated by SwissParam using CHARMM all atoms force field [35]. Subsequently, the atom types in the topology files were modified as per the standard CHARMM27 atom types applicable to nucleotide bases. The complexes were solvated using Simple Point Charge (SPC) water molecules in an octahedron box with periodic boundary conditions and the system was neutralized by adding counter ions.

Long-range electrostatics were calculated using Particle Mesh Ewald (PME) summation with 10 Å cut-off for columbic interactions [36]. The short-range electrostatic and van der Waals distance cut-off was set to 1.1 nm and 1.4 nm, respectively. The system was energy minimized using the steepest descent algorithm with a tolerance of 1000 kJ mol^{-1} nm^{-1}. The atomic positions of the complexes were restrained and the system was equilibrated in NVT (isochoric-isothermal; for 1 ns) followed by NPT (isobaric-isothermal; for 2 ns) ensemble, where the temperature and pressure were maintained at 300 K and 1.05 bar, respectively. Modified Berendsen thermostat [37] and Parinello-Rahman [38] barostat methods were used to stabilize the temperature and pressure, respectively. After equilibrating the system, the position restraints were released and subjected to 100 ns (50 million steps) of production run using a time step of 2 fs? The frames were saved every 1000 steps and the resultant MD trajectories were analyzed using ngmx (GROMACS trajectory viewer) and xmgrace ver. 5.1.2.

2.6.1. Calculation of interaction energies

To quantify the strength of protein-aptamers association, the average non-bonded interaction energies $\langle E^{int} \rangle$ from the simulation of the complexes beyond 10 ns was calculated as per equation (2).

$$\left\langle E^{int} \right\rangle = \langle LJ \rangle + \langle Coul \rangle \quad (2)$$

Where ⟨⟩ denotes the average energy values (Kcal/mol) obtained from the MD trajectories. *LJ* and *Coul* denote the short-range Lennard–Jones and Coulomb interaction energies, respectively. The average short-range *LJ* and *Coul* interaction energies between the HER2(ECD) residues and aptamers were computed using the g_energy tool of GROMACS.

2.6.2. Cluster analysis

Cluster analysis was performed for all the MD trajectories (10 ns-100 ns time period) using Gromos method [39]. The backbone atoms RMSD cut-off value was chosen such that the total clusters obtained from each trajectory would be ≤ 100 [40]. An average structure (also termed as a centroid or a dominant conformation), representative of each cluster was extracted, and a collection of all

Table 2
Docking results and cluster analysis performed for the HADDOCK generated WRMs of HER2-aptamers complexes.

Aptamer (docked to HER2(ECD))	Total no. of WRMs retrieved (*a*)	Total no. of clusters obtained	Size of the largest cluster (*b*)[a]	Mean HADDOCK score of the largest cluster
H1	162	11	67 (41.3)	−57.5 ± 3.7
H2	143	13	66 (46.1)	−47.1 ± 5.5
H3	167	10	49 (29.3)	−45.6 ± 4.8
H4	169	7	90 (53.2)	−45.5 ± 3.9
H5	167	8	54 (32.3)	−37.1 ± 5.9
H6	177	10	75 (42.3)	−44.7 ± 6.8
H7	151	14	45 (29.8)	−64.9 ± 5.2
Poly T	160	11	59 (36.8)	−38.6 ± 2.7

[a] Decimal numbers in the parenthesis indicate percentage of WRMs contribute to the largest cluster with respect to the total number of HADDOCK generated WRMs. It is calculated by using formula, b × 100/a.

the average structures constituted an ensemble. All the structural illustrations were prepared using LigPlot + ver. 1.4.5, PyMOL (Schrödinger, LLC. (2010)) and the UCSF Chimera package [41].

3. Results

3.1. Elucidation of putative aptamer binding sites on HER2(ECD)

DISPLAR [27] and DNABINDPROT [28] revealed the key amino acids that are potential DB residues of HER2(ECD) protein. These residues are identified as, Gly30, Gln32, Val34, Asn37, Leu38, Gln53, Asp54, Gln56, Gly60, Tyr61, Val62, Leu63, Arg76, Val80, Gly82, Leu85, Phe86, Ala91, Leu92, Leu95, Gln404, Asn405, Arg434, and Ser435. The relative positions of these residues on the HER2(ECD) are highlighted as-*Sites* 1a, 1 b, 2a and 2 b in Fig. 1(a). Further, the continuum surface electrostatics plays a crucial role in protein-nucleic acids interactions. The HER2(ECD) structure had a global net charge of −13 at pH 7.4, while a quantum of positive charge was found localized on the *Site* 2 (Fig. 1(b)). Nonetheless, the residues represented *Sites* 1a and 1 b, as well as 2a and 2 b were assigned as active residues for docking (see Materials and Methods). The structures of ssDNA aptamer variants were modeled as described in the methods. Additionally, the structure of modeled poly T -a non-specific oligo sequence, was used as a negative control for the purpose of *in silico* validation, since it did not bind to the HER2 protein during the *in vitro* SELEX process [26].

3.2. HER2(ECD) residues which harbor aptamers binding are identified by docking studies

To elucidate the binding modes of anti-HER2 aptamer variants (Table 1) and residues crucial for binding, docking simulations were carried out. The 3D structures of all the eight aptamer variants (H1-H7 and poly T) were modeled and docked to the HER2(ECD) protein structure. After each docking exercise, cluster analysis was performed for a maximum of 200 WRMs generated in the final stage of the HADDOCK docking protocol. Several clusters were generated using a pair-wise backbone root mean square deviation (rmsd) cut-off of 7.5 Å and a minimum cluster size of 4 (default values) as the criteria. These clusters were then ranked on the basis of HADDOCK scores calculated using weighted intermolecular energy terms. The best model belonged to the largest cluster, which was chosen as a representative of each docking run. Results of cluster analysis with total eight docking runs are shown in Table 2.

Of the eight largest clusters, the clusters belonging to H1, H2, and H7 had lowest mean HADDOCK scores and therefore, these three could exhibit higher affinity for HER2(ECD). Among these three truncated aptamers, the largest clusters pertaining to H1 and H2 (with the mean HADDOCK scores of -57.5 ± 3.7 and -47.1 ± 5.5, respectively), represented 41.3% and 46.1%, respectively of the total number of WRMs generated by the HADDOCK protocol. Whereas, in case of H7 (best mean HADDOCK score), the largest cluster represented only 29.8% of the total number of WRMs. On the other hand, H4 and H6 docking resulted in the clusters with the largest populations (90 and 75 WRMs respectively) as compared to the remaining clusters with reasonable mean HADDOCK scores (see Table 2). Among all, HER2(ECD)-H5 and poly T docking resulted in clusters with poor HADDOCK scores and hence, H5 and poly T oligomers may exhibit weak binding affinities towards HER2(ECD). Further, the representative docked models selected from the largest clusters obtained from seven independent docking exercises were analyzed. The models were investigated to delineate the binding modes of the aptamers and HER2(ECD) residues crucial for binding. All of the *in vitro* selected aptamers bind to the predicted DB *Site* 2a of HER2(ECD) and their binding modes are illustrated in Fig. 2.

Structural analysis of docked complexes indicated that, apart from hydrophobic interactions, all of the aptamers interacted with HER2 protein by forming salt bridges with at least one basic Aptamer Interacting Residue (AIR) except H5 and H3 aptamers (Table S1). AIRs which harbor ssDNA aptamers through hydrogen bond and electrostatic interactions are shown in Table S1. We also studied the relative frequency of these interactions made by the

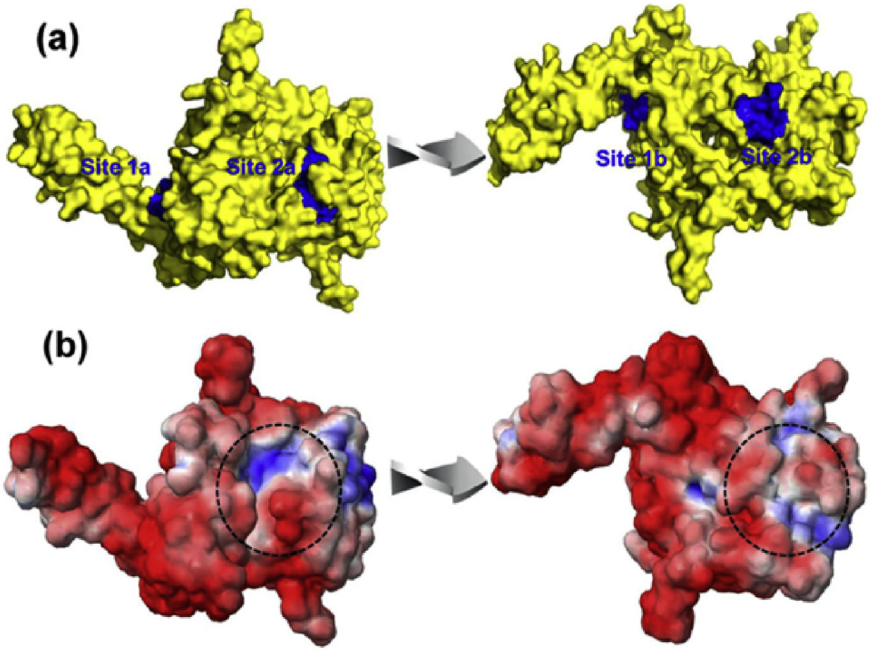

Fig. 1. Assessment of potential DB regions in HER2(ECD). (a) Surface representations of HER2(ECD) showing potential DB residues/regions (blue color) predicted by DISPLAR and DNABINDPROT servers. (b) The electrostatic solvent assessable surface potential of HER2(ECD) solvent accessible surface is depicted at −5 kT/e (in red) and +5 kT/e (blue) using JmolApplet. Positively charged electrostatic potentials found at the predicted DB Sites 2a and 2 b of HER2(ECD) are encircled.

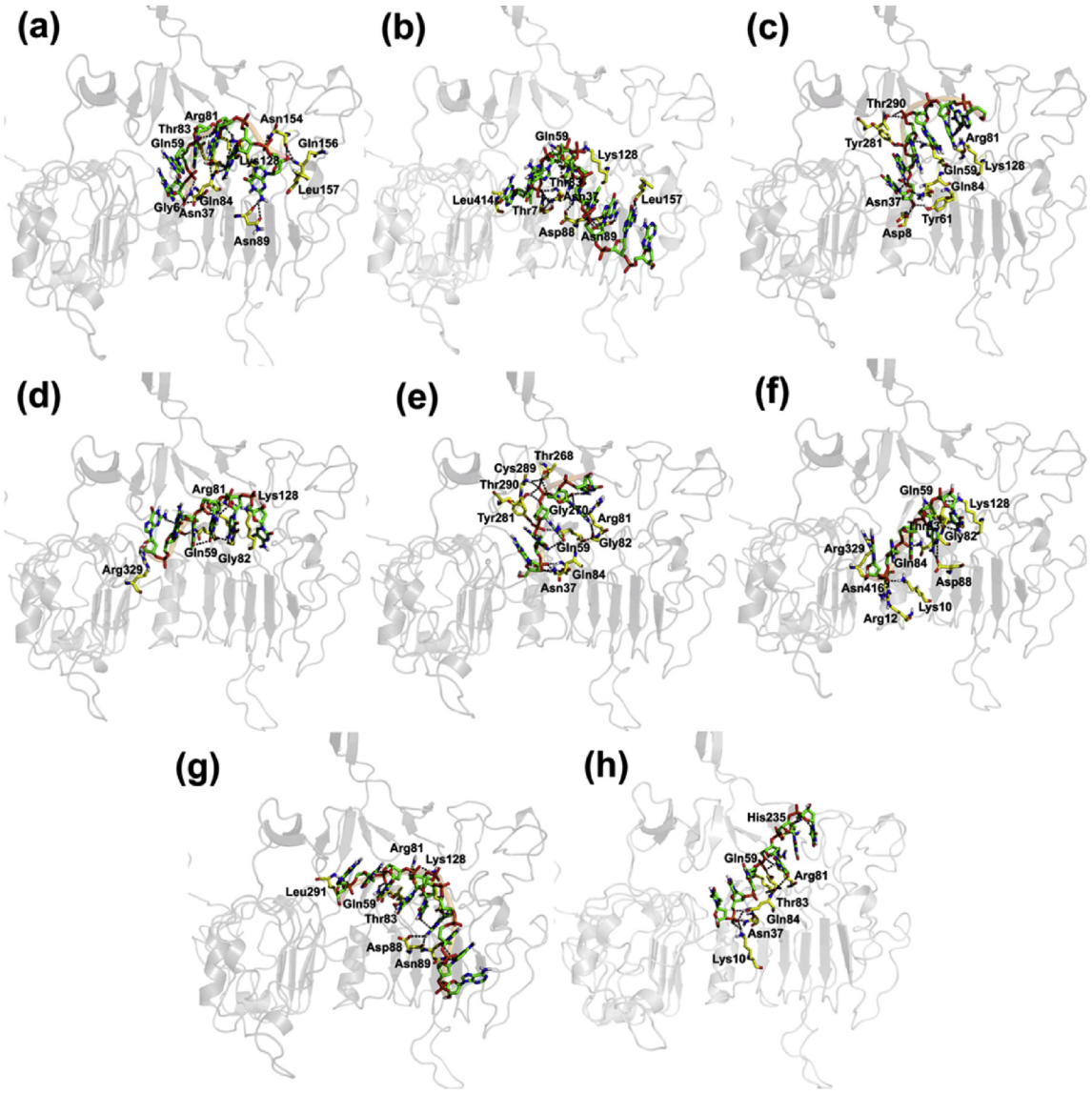

Fig. 2. Depiction of the representative aptamers poses (a) H1 (b) H2 (c) H3 (d) H4 (e) H5 (f) H5 (g) H7 and (h) Poly T obtained after docking to HER2(ECD). AIRs belonged to *Site* 2a of HER2(ECD) are shown as yellow carbon sticks while the aptamers are shown as green carbon sticks. HER2(ECD) is shown as a transparent gray cartoon while polar contacts are shown as dashed lines. (For interpretation of the references to color in this figure legend, the reader is referred to the Web version of this article.)

HER2 AIRs with aptamers in all docked complexes. It was found that the positively charged AIRs, such as Lys128 and Arg81 had the highest frequencies (14 and 8, respectively) (Fig. S4). This implies that the electrostatic interactions play an important role in high-affinity aptamer binding. Further, polar HER2-AIRs *viz.* Gln59, Gln84, Thr83, Asn37 and Asp88 frequently engaged with the aptamers via hydrogen bond contacts (Fig. 3 and Fig. S4). Other residues such as Gly82, Asn89, Lys10, Arg12, Asn154, Gly270, Tyr281, Thr289, and Arg329 were less frequently involved in the formation of hydrogen bond contacts with the aptamers albeit their contribution to the high-affinity binding cannot be undermined.

3.2.1. Validation of HADDOCK ver. 2.1 protocol for protein-aptamer docking

The HADDOCK ver. 2.1 protocol was validated by re-docking the high-resolution X-ray co-crystal structures of cognate and non-cognate ssDNA aptamers (9mers) complexed with the Protection of telomeres protein 1 (Pot1pC) (PDB id: 4HIK, 4HID, 4HIM, 4HIO, 4HJ5, 4HJ7 and 4HJ8) [42]. These complexes were selected since the length of the aptamers sequences (9mers) was less than ten bases. Additionally, unavailability of the co-crystal structures of HER2(ECD) protein complexed with anti-HER2 aptamers prompted us to use the above high-resolution co-crystal structures; as these may be considered ideal for the validation of docking protocol for at least in the present case. The protein component of the complex (PDB id: 4HIK) was prepared using the Prepare Protein protocol of DS. 3.5. The aptamer component of all the seven PDB structures listed above was protonated and their geometry was optimized by energy minimization keeping parameters identical to that used for anti-HER2 aptamer models. Prior to docking, the DNA binding hot spots present on the Pot1pC protein was investigated by means of continuum electrostatic surface potential maps. As expected, the DNA binding hot-spot on the Pot1pC protein is amongst the regions localized with most positive charge and the global net charge on the protein was found to be +1, as observed at pH 7.4 (Fig. S5). The aptamer binding hot spot regions encompassing the residues, *viz.* Lys25-Tyr28, Lys31-Tys36, Phe47-Ser50, Thr53-Trp58, Arg68-Asp73, Lys97-Leu101

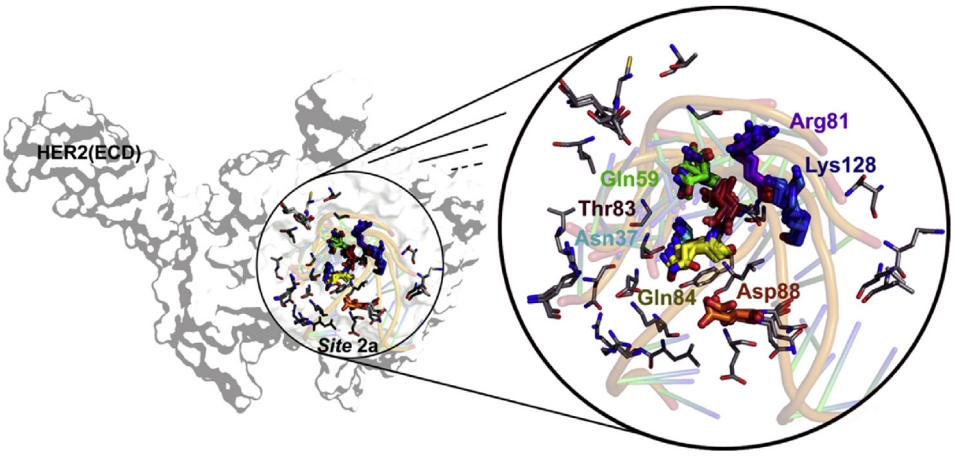

Fig. 3. Molecular overlay of representative HADDOCK generated water refined models of HER2(ECD)-aptamers (H1-H7) complexes. HER2(ECD) protein and the docked aptamers are shown as transparent cartoon representations. AIRs forming contacts to the aptamers are highlighted. Important AIRs which form minimum contact frequency of four, as observed in all representative-docked structures are labeled.

and Tyr103-Gly110 were defined as the actives while re-docking the co-crystallized aptamers.

The validation involved comparison of the heavy atoms root-mean-square deviation (rmsd) calculated for the re-docked aptamers' poses with respect to the corresponding poses of the aptamers co-crystallized with the Pot1pC protein. A threshold of 2 Å rmsd or less is widely accepted as standard value to distinguish the success/failure of a docking protocol to reproduce the binding mode [43]. In the present case, rmsd calculated between the heavy atoms of docked and co-crystallized aptamer poses was found to be < 2 Å. This indicates that the docking protocol correctly reproduced the experimental binding poses of the aptamers (see Fig. 4 for structural illustrations). The overall *in vitro* profile of Pot1pC binding ssDNA aptamers and their docking results are shown in Table S2.

3.3. MD simulations revealed H1, H2, and H6 forms stable complexes with HER2(ECD) protein

To study the stability of HADDOCK generated representative models of H1, H2, H6 and poly T aptamers complexed with HER2(ECD), 100 ns of MD simulations were carried out. The former three complexes were selected amongst the seven (H1-H7) because, the aptamers *namely*, H1, H2 and H6 exhibited highly specific *in vitro* HER2 protein binding property and therefore, evolved multiple times during the combinatorial iterative selection process of SELEX [26]. Whereas the latter was selected for the purpose of *in silico* validation since the nonspecific poly T aptamer neither evolved during *in vitro* SELEX process nor displayed HER2(ECD) binding property. Therefore, poly T aptamer could be considered as a negative control. The geometrical features such as, backbone rmsd, radius of gyration (Rg), distance between the center of mass of the interacting species, intermolecular hydrogen bonds, solvent accessible surface area (SASA) and the average residue-wise root mean square fluctuations (rmsf) were assessed for all trajectories and the resultant graphs are plotted as shown in Fig. 5(a–f).

The rmsd plots (Fig. 5(a)) revealed that the complexes, HER2(ECD)-H1 and -H2 attained stability past 23 ns with a slight drift in rmsd during 80 ns? The average rmsd values calculated for HER2(ECD)-H1 and -H2 complexes were found to be 1.31 nm and 1.28 nm, respectively. The HER2(ECD)-H6 complex displayed slight conformational distortions at ~25 ns and 40 ns? Overall, the complex showed lesser structural deviations with respect to the initial structure throughout the simulation time with an average rmsd of 0.67 nm. This trend was not observed in case of HER2(ECD)-poly T since the complex displayed higher conformational instability throughout the simulation time with a maximum rmsd of 3.5 nm (Fig. 5(a)). The Rg plots showed no significant deviations when compared with the average Rg values calculated for HER2 aptamer interacting residues (AIRs)-H1 (0.94 nm), -H2 (1.08 nm) and -H6 (0.67 nm) trajectory frames. However, the HER2-poly T complex exhibited a steep rise in the Rg values until ~60 ns, and later, an unsteady trend was observed throughout the course of MD simulation. This implies that the HER2-poly T complex is loosely packed and relatively unstable (Fig. 5(b)). Other parameters such as distance and H bonds were computed between HER2 AIR atoms and the aptamers and plotted as a function of time. AIRs are the HER2(ECD) residues that are directly involved in the interactions with the aptamers as observed in the representative docked models, see Table S1.

The trend of intermolecular distances throughout the course of MD simulations differed considerably between the complexes, as seen in Fig. 5(c). However, the average distance calculated between the center of mass of HER2(AIR) and H1, and likewise for H2 and H6 were found to be roughly same (i.e. 1.30 nm, 1.085 nm, and 1.051 nm, respectively). Whereas, the average distance computed between the HER2(AIRs) and poly T was approximately twice as compared to the former three complexes (2.24 nm). The deviations in the distance between the aptamers and HER2(AIRs) during the course of simulations had a direct influence on the magnitude of intermolecular H bond contacts, as seen in Fig. 5(d). We observed that, on an average, H1, H2, and H6 formed 2, 4 and 2H bonds, respectively with the HER2(AIRs).

Unlike the H1, H2, and H6 aptamers, poly T formed the least number of H bond interactions with the HER2(AIRs) and therefore, showed a weak association with the HER2 protein. Furthermore, the total SASA of HER2(AIRs) in all the trajectories was evaluated to study the relative trend of solvent accessibility throughout the course of MD simulations (Fig. 5(e)). In general, the higher the solvent accessibility, the lesser will be interactions of AIRs with the aptamers.

The H1, H2, and H6 interacting residues maintained a constant trend of SASA (<20 nm^2) till the end of simulations. Therefore, H1, H2, and H6 aptamers displayed higher binding affinity towards HER2 protein. Whereas, poly T interacting residues had higher solvent accessibility (~23 nm^2) and therefore, showed less number of interactions with the poly T aptamer

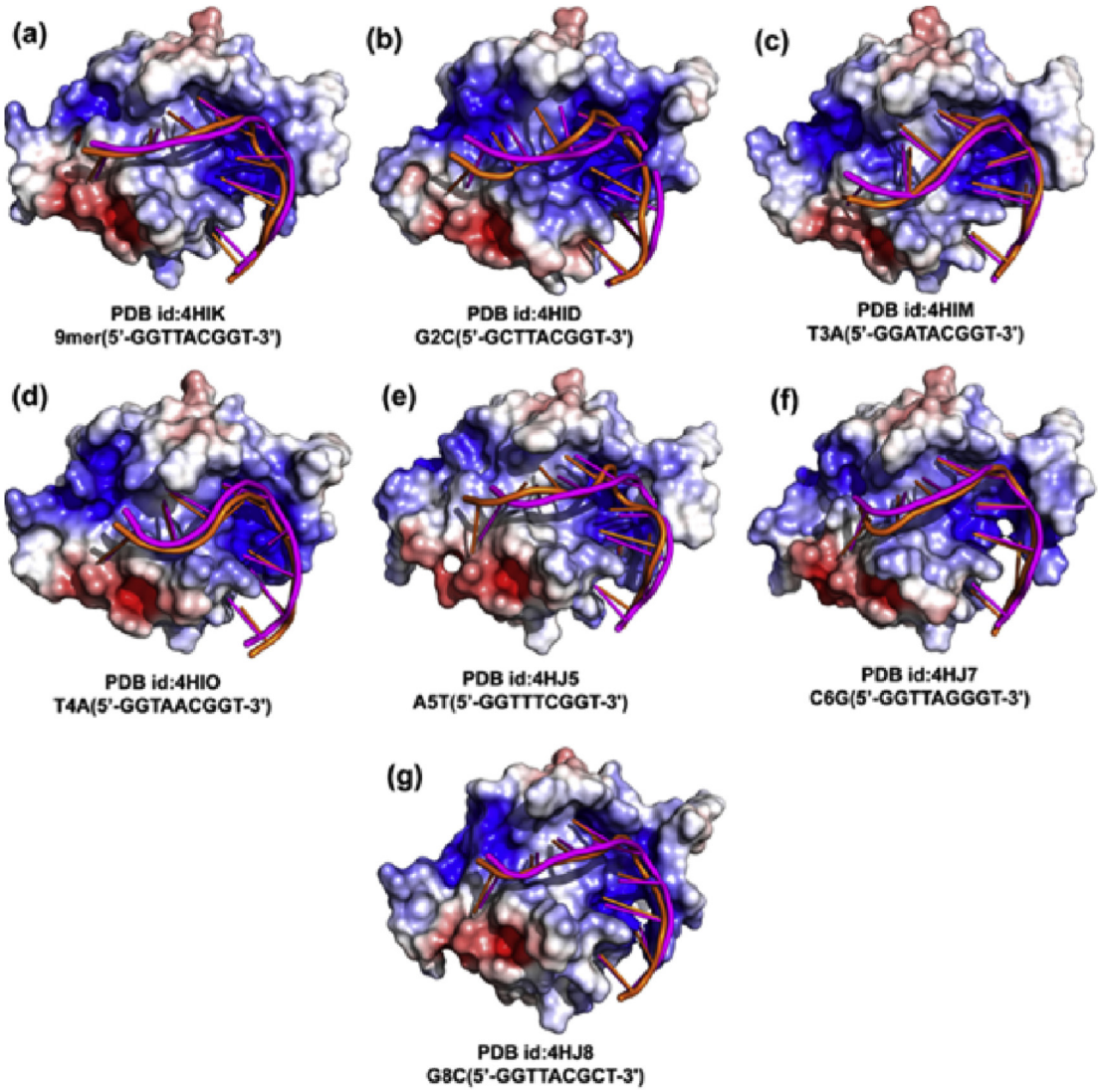

Fig. 4. Superposition of HADDOCK representative docked models (orange color cartoon representations) with co-crystal structures of Pot1pC-aptamer (magenta color cartoon representations) complexes. The electrostatic potentials on the solvent accessible surface of Pot1pC protein are generated from ABPS tools. (For interpretation of the references to color in this figure legend, the reader is referred to the Web version of this article.)

until the end of the simulation time. The residue-wise average RMSF plots revealed the high flexible regions of HER2(ECD) such as, Gly98-Gly114, Ala169-Cys182, Cys316-Gly322 and Phe349-Pro369 which are the loops interconnecting the HER2(ECD) sub-domains, also includes the region, Leu244-Tyr267 corresponded to the dimerization loop of sub-domain II (see Fig. 5(f)). The extent of the fluctuations of the above regions differed considerably in all trajectories. Apart from these regions, the average RMSF of HER2 residues was assessed in all MD trajectories to study the effect of aptamer binding on protein conformational stability. The RMSF graphs indicated that the backbone and side chain atoms corresponded to the loop regions of HER2(ECD) bound to poly T displayed higher fluctuations as compared to that in the remaining cases during 100 ns of MD simulations. Interestingly, poly T AIRs displayed lower fluctuations during MD simulations. This is due to the stabilizing interresidue interactions that restrict the conformational freedom rather because of aptamer binding. Unlike poly T AIRs, H1, H2, and H6 AIRs showed relatively more fluctuations during MD simulations revealing their high preference for H1, H2, and H6 aptamers.

3.3.1. Structural analysis and interaction energy calculations revealed H1, H2, and H6 aptamer variants have greater propensities for binding to the HER2 protein as compared to poly T

The complexes undergoing dynamical changes during MD simulations were interrogated to delineate the relative propensities of the aptamers for HER2 protein. Clustering of trajectory structures saved during MD simulations of the HER2(ECD)-H1, H2, H6 and poly T complexes resulted in 10, 10, 04 and 11 clusters, respectively. The information about average structures along with the sizes of the populations constituting the clusters and ensembles of average structures are shown in Figs. S6,S7,S8,S9. The average structures and their ensembles were examined to assess the HER2(ECD) bound aptamers amenable for conformational changes during MD simulations. We found that the largest clusters obtained from the cluster analysis of HER2(ECD)-H1, H2, H6 and poly T trajectories constituted ~73%, 79%, 98% and 71%, respectively of the total populations sampled during MD simulations. We observed that aptamers, H1 and H2 showed greater propensities for HER2(ECD) as evident from Rg, distance and total SASA plots (Fig. 5(b), (c) and (e)), which is attributable to the minimal conformational deviations during MD simulations (Figs. S6 and S7). H6 aptamer exhibited four

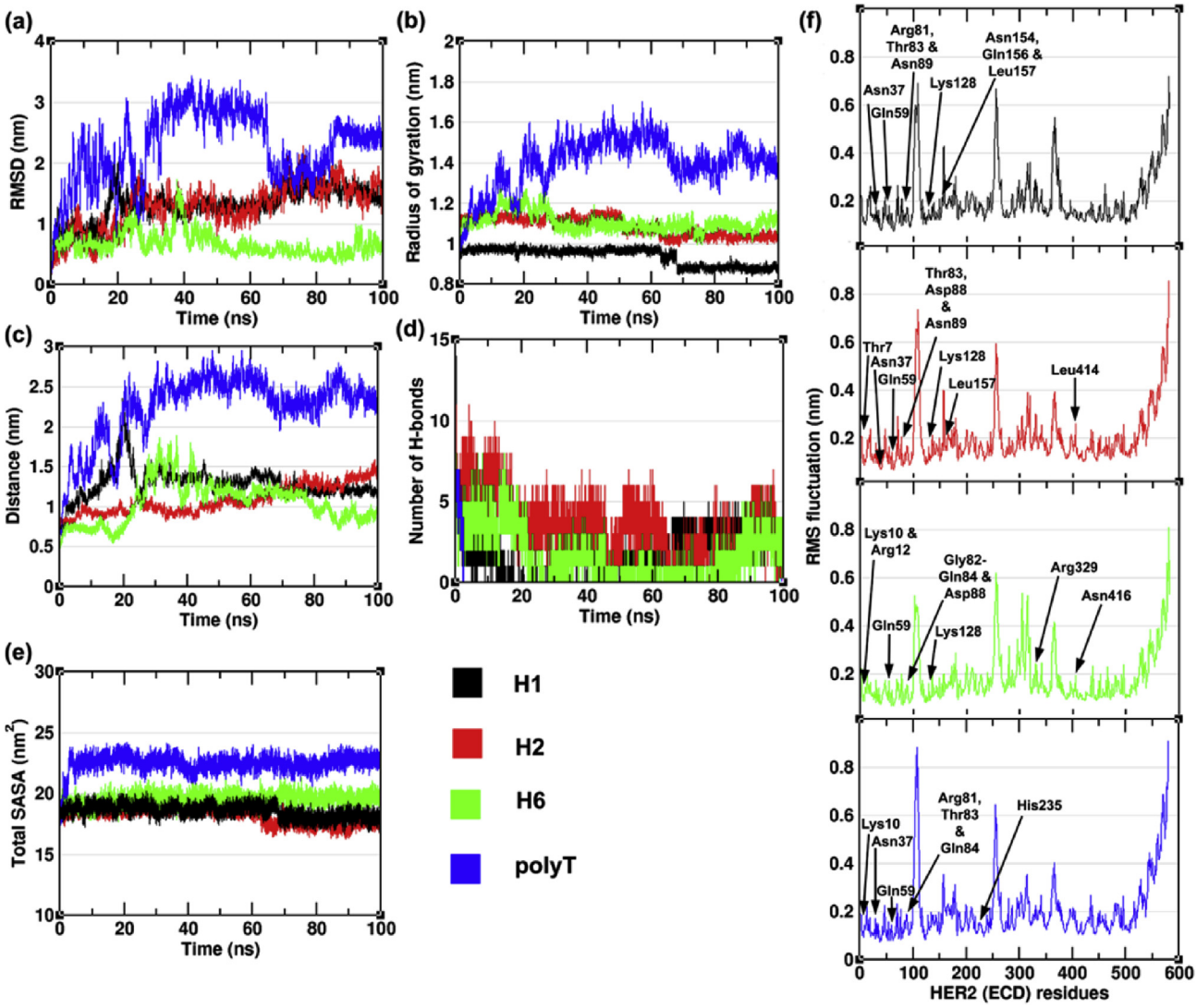

Fig. 5. Analysis and comparison of MD geometrical features *viz.* (a) rmsd, (b) Rg, (c) Distance, (d) number of H-Bonds (e) Total SASA plotted as a function of time and (f) Residue wise average rmsf of HER2(ECD) residues to assess the binding stability of H1, H2, H6 and poly T-HER2(ECD) complexes using MD trajectories. AIRs identified from the docking analysis are labeled.

distinct binding conformations of which the first conformation is an average of the largest cluster having 98.80% of the total sample population (Fig. S8). On the contrary, the least binding stability of poly T and its propensity for the HER2(ECD) may be attributed to the high conformational fluctuations and poor stability as a result of least number of stabilizing non-covalent intermolecular interactions (Fig. S9).

Furthermore, structural assessment of the average structures also indicated the aptamers H1, H2, and H6 formed higher non-bonded interactions (preferably electrostatic and H bond interactions with the AIRs), whereas, poly T formed the least (See Fig. 6). The average non-bonded interaction energy, $\langle E^{int} \rangle$ which gives an approximation to gauge the binding affinity, was calculated for all the frames of MD trajectories. The $\langle E^{int} \rangle$ values calculated specifically between HER2(ECD) and the aptamers were found to be highly favorable for H1, H2, and H6 aptamers, and least for poly T. The favorable interaction energies (in Kcal/mol) were in the order, H2 (−124.0)>H1 (−109.0)>H6 (−99.0)>ploy T (−45.0). Further analysis revealed that a major contribution to overall non-bonded interaction energy, E^{int} comes from the *Coul* term, while the remaining from *LJ* term. Here, both *Coul* and *LJ* terms refer to the energetic and steric components of protein-aptamer complex formation, which also contribute for binding specificity (Fig. 7). On the other hand, the mean HADDOCK scores of the aptamers obtained from the docking were in the order of H1 (-57.5 ± 3.7)>H2 (-47.1 ± 5.5)>H6 (-44.7 ± 6.8)>poly T (-38.6 ± 2.7). While the H1 aptamer exhibited a better mean HADDOCK score, the largest cluster of WRMs pertaining to H2 represented the highest percentage (46.1%) of the total number of WRMs generated. Additionally, the dissociation constant (K_d) for H2 according to one-site binding assay was calculated to be 270 nM against the target 300 nM HER2 protein present in the reaction mixture. Which means, ~1:1 stoichiometric molecular binding occurred with H2 ssDNA-to-HER2 protein [26].

An overview of all the studied parameters indicated that the anti-HER2 aptamers, viz. H1, H2, and H6 displayed the greater binding propensity for the HER2 receptor; of which, H2 exhibited most favorable interaction energy and conformational stability. Whereas, poly T showed the weak binding propensity and least conformational stability according to both docking and MD simulation studies; consistent with the observations wherein, poly T failed to evolve during the *in vitro* SELEX process. These results are

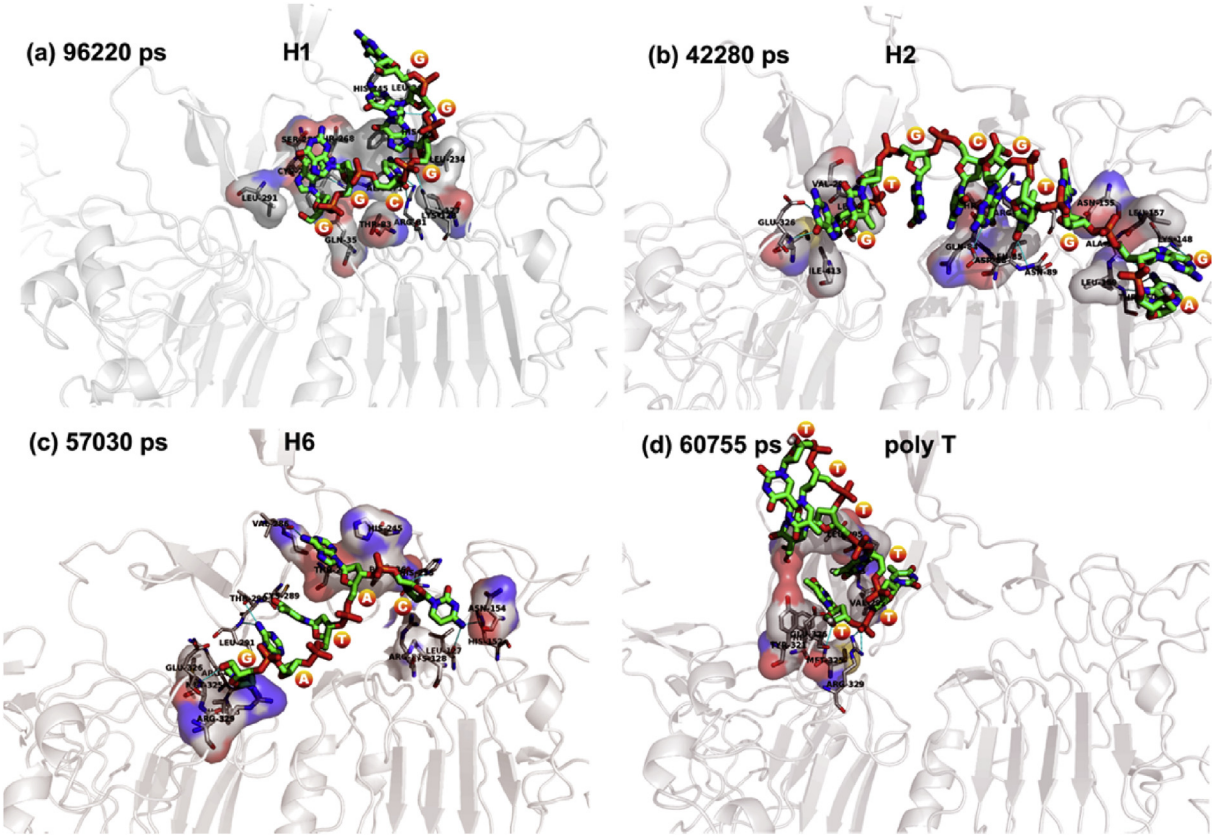

Fig. 6. Analysis of protein-aptamer interactions in the representative average structures extracted from largest clusters of the MD frames of each trajectory. (a) HER2(ECD)-H1, (b) HER2(ECD)-H2, (c) HER2(ECD)-H6 and (c) HER2(ECD)-poly T complexes. H bonds are shown as cyan lines. (For interpretation of the references to color in this figure legend, the reader is referred to the Web version of this article.)

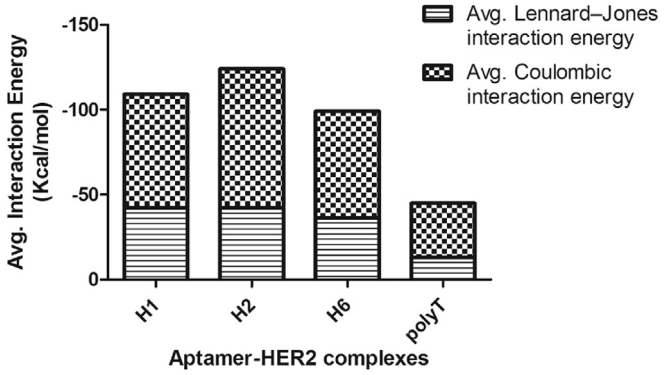

Fig. 7. Histograms representing the average non-bonded interaction energies calculated specifically between HER2(ECD) and the aptamers.

in fact interesting because the MD simulations were performed using explicit SPC waters, which form a non-default solvent model for simulations using the CHARMM27 force field. Notwithstanding, an independent MD simulation study using default water model (TIP3P) is warranted to derive the subtle changes that occur due to the salvation of charged residues; and its overall implication in protein-aptamer interactions and dynamics.

4. Conclusion

In conclusion, our detailed retrospective investigation approach involving the *in vitro* anti-HER2 aptamers selection process followed by *in silico* structural analysis and molecular docking simulations revealed HER2(ECD) residues, primarily those of Site 2a viz. Lys128, Arg81, Gln59, Gln84, Thr83, Asn37, and Asp88 harbor anti-HER2 aptamers binding. Further, six anti-HER2 aptamers whose largest clusters had the mean HADDOCK scores higher than −40 follow the rank order of H7>H1>H2>H3≈H4>H6. Though H7 and H3 have favorable mean HADDOCK scores which corresponded to the largest clusters that represented less than 30% of the total number of WRMs generated as opposed to >40% as in the cases of H1, H2, H4, and H6. Of the eight, HER2(ECD)-H5 and poly T (negative control) docking resulted in clusters with poor mean HADDOCK scores. Of the four (H1, H2, H4, and H6), three HER2-aptamer complexes viz. H1, H2, and H6 were further shortlisted for MD simulation studies because apart from having favorable HADDOCK scores, they also evolved multiple times through the *in vitro* SELEX process. MD simulations have indicated that HER2(ECD)-H2 complex displayed greater conformational stability and most favorable interaction energy, which is followed by H1 than H6. On the contrary, HER2(ECD)-poly T complex exhibited the least stability. These findings are in agreement with our previous *in vitro* study [26], wherein, H1, H2, and H6 anti-HER2 aptamers were evolved multiple times through the wet-lab SELEX process, inferring their higher binding preference for HER2 protein. The knowledge of aptamer binding features garnered from this study could be complemented with affinity maturation [44] which could further guide the development of better anti-HER2 aptamers for future cancer therapeutic and/or diagnostic applications.

Conflicts of interest

The authors declare that they have no conflict of interest.

Acknowledgments

The authors are grateful to Dr. Smita D. Mahale (Director, NIRRH, Mumbai), Dr. Susan Idicula-Thomas (Scientist D, NIRRH, Mumbai) and Principal, JSS College of Pharmacy, Mysuru for all the assistance and support. The authors also thank Ms. Faiza Hanif Waghu for the support during MD simulations. Sarfaraj Niazi thanks the Indian Council of Medical Research (ICMR), Ansari Nagar, New Delhi, for the award of Senior Research Fellowship (SRF), Ref. No. BIC/11(16)/2014 & IRIS ID No. 2014–23020.

Appendix A. Supplementary data

Supplementary data related to this article can be found at https://doi.org/10.1016/j.jmgm.2018.06.003.

References

[1] J. Schlessinger, Cell signaling by receptor tyrosine kinases, Cell 103 (2000) 211–225, https://doi.org/10.1016/S0092-8674(00)00114-8.
[2] R.N. Jorissen, F. Walker, N. Pouliot, et al., Epidermal growth factor receptor: mechanisms of activation and signalling, Exp. Cell Res. 284 (2003) 31–53, https://doi.org/10.1016/S0014-4827(02)00098-8.
[3] A.W. Burgess, H.-S. Cho, C. Eigenbrot, et al., An open-and-shut Case? Recent insights into the activation of EGF/ErbB receptors, Mol. Cell 12 (2003) 541–552, https://doi.org/10.1016/S1097-2765(03)00350-2.
[4] R. Landgraf, R. Nahta, F. Esteva, et al., HER2 therapy. HER2 (ERBB2): functional diversity from structurally conserved building blocks, Breast Cancer Res. 9 (2007) 202, https://doi.org/10.1186/bcr1633.
[5] I. Rubin, Y. Yarden, The basic biology of HER2, Ann. Oncol. 12 (2001) S3–S8, https://doi.org/10.1093/annonc/12.suppl_1.S3.
[6] Y. Yarden, Biology of HER2 and its importance in breast cancer, Oncology 61 (2001) 1–13, https://doi.org/10.1159/000055396.
[7] M.A. Lemmon, J. Schlessinger, I. Amit, et al., Cell signaling by receptor tyrosine kinases, Cell 141 (2010) 1117–1134, https://doi.org/10.1016/j.cell.2010.06.011.
[8] D. Harari, Y. Yarden, Molecular mechanisms underlying ErbB2/HER2 action in breast cancer, Oncogene 19 (2000) 6102–6114, https://doi.org/10.1038/sj.onc.1203973.
[9] D.J. Slamon, W. Godolphin, L.A. Jones, et al., Studies of the HER-2/neu proto-oncogene in human breast and ovarian cancer, Science 244 (1989) 707–712, https://doi.org/10.1126/science.2470152.
[10] M.C. Hung, A. Matin, Y. Zhang, et al., HER-2/neu-targeting gene therapy–a review, Gene 159 (1995) 65–71.
[11] W. Xia, R.J. Mullin, B.R. Keith, et al., Anti-tumor activity of GW572016: a dual tyrosine kinase inhibitor blocks EGF activation of EGFR/erbB2 and downstream Erk1/2 and AKT pathways, Oncogene 21 (2002) 6255–6263, https://doi.org/10.1038/sj.onc.1205794.
[12] E.R. Wood, A.T. Truesdale, O.B. McDonald, et al., A unique structure for epidermal growth factor receptor bound to GW572016 (Lapatinib): relationships among protein conformation, inhibitor off-rate, and receptor activity in tumor cells, Canc. Res. 64 (2004) 6652–6659, https://doi.org/10.1158/0008-5472.CAN-04-1168.
[13] D.W. Fry, A.J. Bridges, W.A. Denny, et al., Specific, irreversible inactivation of the epidermal growth factor receptor and erbB2, by a new class of tyrosine kinase inhibitor, Proc. Natl. Acad. Sci. U. S. A. 95 (1998) 12022–12027.
[14] H.-R. Tsou, E.G. Overbeek-Klumpers, W.A. Hallett, et al., Optimization of 6,7-disubstituted-4-(arylamino)quinoline-3-carbonitriles as orally active, irreversible inhibitors of human epidermal growth factor receptor-2 kinase activity, J. Med. Chem. 48 (2005) 1107–1131, https://doi.org/10.1021/jm040159c.
[15] K. Yokoi, P.H. Thaker, S. Yazici, et al., Dual inhibition of epidermal growth factor receptor and vascular endothelial growth factor receptor phosphorylation by AEE788 reduces growth and metastasis of human colon carcinoma in an orthotopic nude mouse model, Canc. Res. 65 (2005) 3716–3725, https://doi.org/10.1158/0008-5472.CAN-04-3700.
[16] F.A.L.M. Eskens, C.H. Mom, A.S.T. Planting, et al., A phase I dose escalation study of BIBW 2992, an irreversible dual inhibitor of epidermal growth factor receptor 1 (EGFR) and 2 (HER2) tyrosine kinase in a 2-week on, 2-week off schedule in patients with advanced solid tumours, Br. J. Canc. 98 (2008) 80–85, https://doi.org/10.1038/sj.bjc.6604108.
[17] T.W. Wong, F.Y. Lee, C. Yu, et al., Preclinical antitumor activity of BMS-599626, a pan-HER kinase inhibitor that inhibits HER1/HER2 homodimer and heterodimer signaling, Clin. Canc. Res. 12 (2006) 6186–6193, https://doi.org/10.1158/1078-0432.CCR-06-0642.
[18] M.G. Kris, R.B. Natale, R.S. Herbst, et al., Efficacy of gefitinib, an inhibitor of the epidermal growth factor receptor tyrosine kinase, in symptomatic patients with non–small cell lung cancer, J. Am. Med. Assoc. 290 (2003) 2149, https://doi.org/10.1001/jama.290.16.2149.
[19] J.P. Jani, R.S. Finn, M. Campbell, et al., Discovery and pharmacologic characterization of CP-724,714, a selective ErbB2 tyrosine kinase inhibitor, Canc. Res. 67 (2007) 9887–9893, https://doi.org/10.1158/0008-5472.CAN-06-3559.
[20] M.C. Franklin, K.D. Carey, F.F. Vajdos, et al., Insights into ErbB signaling from the structure of the ErbB2-pertuzumab complex, Canc. Cell 5 (2004) 317–328.
[21] H.-S. Cho, K. Mason, K.X. Ramyar, et al., Structure of the extracellular region of HER2 alone and in complex with the Herceptin Fab, Nature 421 (2003) 756–760, https://doi.org/10.1038/nature01392.
[22] H. Zhou, Z. Zha, Y. Liu, et al., Structural insights into the down-regulation of overexpressed p185(her2/neu) protein of transformed cells by the antibody chA21, J. Biol. Chem. 286 (2011) 31676–31683, https://doi.org/10.1074/jbc.M111.235184.
[23] R.D. Fisher, M. Ultsch, A. Lingel, et al., Structure of the complex between HER2 and an antibody paratope formed by side chains from tryptophan and serine, J. Mol. Biol. 402 (2010) 217–229, https://doi.org/10.1016/j.jmb.2010.07.027.
[24] C. Eigenbrot, M. Ultsch, A. Dubnovitsky, et al., Structural basis for high-affinity HER2 receptor binding by an engineered protein, Proc. Natl. Acad. Sci. U. S. A. 107 (2010) 15039–15044, https://doi.org/10.1073/pnas.1005025107.
[25] C. Jost, J. Schilling, R. Tamaskovic, et al., Structural basis for eliciting a cytotoxic effect in her2-overexpressing cancer cells via binding to the extracellular domain of HER2, Structure 21 (2013) 1979–1991, https://doi.org/10.1016/j.str.2013.08.020.
[26] J.H. Niazi, S.K. Verma, S. Niazi, A. Qureshi, In vitro HER2 protein-induced affinity dissociation of carbon nanotube-wrapped anti-HER2 aptamers for HER2 protein detection, Analyst (Cambridge, U.K.) 140 (2015) 243–249.
[27] H. Tjong, H.-X. Zhou, DISPLAR: an accurate method for predicting DNA-binding sites on protein surfaces, Nucleic Acids Res. 35 (2007) 1465–1477, https://doi.org/10.1093/nar/gkm008.
[28] P. Ozbek, S. Soner, B. Erman, T. Haliloglu, DNABINDPROT: fluctuation-based predictor of DNA-binding residues within a network of interacting residues, Nucleic Acids Res. 38 (2010) W417–W423, https://doi.org/10.1093/nar/gkq396.
[29] N.A. Baker, D. Sept, S. Joseph, et al., Electrostatics of nanosystems: application to microtubules and the ribosome, Proc. Natl. Acad. Sci. U. S. A. 98 (2001) 10037–10041, https://doi.org/10.1073/pnas.181342398.
[30] T.J. Dolinsky, J.E. Nielsen, J.A. McCammon, N.A. Baker, PDB2PQR: an automated pipeline for the setup of Poisson-Boltzmann electrostatics calculations, Nucleic Acids Res. 32 (2004) W665–W667, https://doi.org/10.1093/nar/gkh381.
[31] M. van Dijk, A.M.J.J. Bonvin, Pushing the limits of what is achievable in protein–DNA docking: benchmarking HADDOCK's performance, Nucleic Acids Res. 38 (2010) 5634–5647, https://doi.org/10.1093/nar/gkq222.
[32] M. van Dijk, A.D.J. van Dijk, V. Hsu, et al., Information-driven protein-DNA docking using HADDOCK: it is a matter of flexibility, Nucleic Acids Res. 34 (2006) 3317–3325, https://doi.org/10.1093/nar/gkl412.
[33] B. Hess, C. Kutzner, D. van der Spoel, E. Lindahl, GROMACS 4: algorithms for highly efficient, load-balanced, and scalable molecular simulation, J. Chem. Theor. Comput. 4 (2008) 435–447, https://doi.org/10.1021/ct700301q.
[34] P. Bjelkmar, P. Larsson, M.A. Cuendet, et al., Implementation of the CHARMM force field in GROMACS: analysis of protein stability effects from correction maps, virtual interaction sites, and water models, J. Chem. Theor. Comput. 6 (2010) 459–466, https://doi.org/10.1021/ct900549r.
[35] V. Zoete, M.A. Cuendet, A. Grosdidier, O. Michielin, SwissParam: a fast force field generation tool for small organic molecules, J. Comput. Chem. 32 (2011) 2359–2368, https://doi.org/10.1002/jcc.21816.
[36] T. Darden, D. York, L. Pedersen, Particle mesh Ewald: an N·log(N) method for Ewald sums in large systems, J. Chem. Phys. 98 (1993) 10089, https://doi.org/10.1063/1.464397.
[37] H.J.C. Berendsen, J.P.M. Postma, W.F. van Gunsteren, et al., Molecular dynamics with coupling to an external bath, J. Chem. Phys. 81 (1984) 3684–3690, https://doi.org/10.1063/1.448118.
[38] S. Nosé, M.L. Klein, Constant pressure molecular dynamics for molecular systems, Mol. Phys. 50 (1983) 1055–1076, https://doi.org/10.1080/00268978300102851.
[39] X. Daura, K. Gademann, B. Jaun, et al., Peptide folding: when simulation meets experiment, Angew. Chem. Int. Ed. 38 (1999) 236–240.
[40] S. Niazi, M. Purohit, Rational design of promiscuous binding modulators of p53 inducing E3(Ub)-ligases (Mdm2 and Pirh2) as anticancer agents: an in silico approach, Medchemcomm 6 (2015) 1959–1968, https://doi.org/10.1039/C5MD00319A.
[41] E.F. Pettersen, T.D. Goddard, C.C. Huang, et al., UCSF Chimera-A visualization system for exploratory research and analysis, J. Comput. Chem. 25 (2004) 1605–1612, https://doi.org/10.1002/jcc.20084.
[42] T.H. Dickey, M.A. McKercher, D.S. Wuttke, et al., Nonspecific recognition is achieved in Pot1pC through the use of multiple binding modes, Structure 21 (2013) 121–132, https://doi.org/10.1016/j.str.2012.10.015.
[43] R.P. Rodrigues, S.F. Andrade, S.P. Mantoani, et al., Using free computational resources to illustrate the drug design process in an undergraduate medicinal chemistry course, J. Chem. Educ. 92 (2015) 827–835, https://doi.org/10.1021/ed500195d.
[44] A.B. Kinghorn, R.M. Dirkzwager, S. Liang, et al., Aptamer affinity maturation by resampling and microarray selection, Anal. Chem. 88 (2016) 6981–6985, https://doi.org/10.1021/acs.analchem.6b01635.